ADVANCED FUNCTIONAL MATERIALS
www.afm-journal.de

Materials Views
www.MaterialsViews.com

Strongly-Coupled Freestanding Hybrid Films of Graphene and Layered Titanate Nanosheets: An Effective Way to Tailor the Physicochemical and Antibacterial Properties of Graphene Film

In Young Kim, Suhye Park, Hyunseok Kim, Sungsu Park, Rodney S. Ruoff, and Seong-Ju Hwang**

An effective way to tailor the physicochemical properties of graphene film is developed by combining colloidal suspensions of reduced graphene oxide (rG-O) nanosheets and exfoliated layered titanate nanosheets for the fabrication of freestanding hybrid films comprised of stacked and overlapped nanosheets. A flow-directed filtration of such mixed colloidal suspensions yields freestanding hybrid films comprised of strongly-coupled rG-O and titanate nanosheets with tunable chemical composition. This is the first example of highly flexible hybrid films composed of graphene and metal oxide nanosheets. The intimate incorporation of layered titanate nanosheets into the graphene film gives rise not only to an increase of mechanical strength but also to increased surface roughness, chemical stability, and hydrophilicity; thus, the physicochemical properties of the graphene film can be tuned by hybridization with inorganic nanosheets. These freestanding hybrid films of rG-O-layered titanate show unprecedentedly high antibacterial property, resulting in the complete sterilization of *Escherichia coli* O157:H7 (≈100%) in the very short time of 15 min. The antibacterial activity of the hybrid film is far superior to that of the pure graphene film, underscoring the beneficial effect of the layered metal oxide nanosheets in improving the functionality of the graphene film.

1. Introduction

Graphene, an exfoliated 2D nanosheet of graphite, attracts intense research interest because of its unique and valuable physicochemical properties such as high electrical conductivity, great mechanical strength, and high flexibility.[1] In contrast to many physical synthetic methods, the soft-chemical exfoliation route enables to prepare the aqueous colloidal suspension of reduced graphene oxide (rG-O) nanosheets, which is fairly suitable for the synthesis of graphene-based nanostructures and nanocomposites.[1b] In one instance, the flow-directed filtration of the colloidal suspension of rG-O makes possible the fabrication of the freestanding films of rG-O featuring a connection by π–π stacking between each carbon monolayers.[2] This graphene freestanding film boasts wide applications as protective layers, chemical filters, components of electrical batteries and capacitor, adhesive layers, molecular storage, and antibacterial or biocompatible matrices.[3,4] However, that this graphene freestanding film is composed of only a carbon element severely limits the tailoring and optimization of its functionality. To overcome this limitation of the graphene film, it is desirable to hybrid with other chemical species. Although many efforts are made to synthesize graphene film hybridized with 0D or 1D inorganic nanostructures,[5] a strong coupling between graphene and inorganic species remains a challenge for enhancing the functionality of the graphene-based freestanding film. Taking into account their extremely high anisotropic 2D morphology and ultrathin thickness (< ≈1 nm), the exfoliated metal oxide nanosheets can be a promising candidate for the formation of homogeneous and strong electronic coupling with graphene nanosheets.[6] Since the exfoliated nanosheets of layered metal oxides possess a wide spectrum of electric, magnetic, and optical properties,[5] the incorporation of these inorganic nanosheets into the graphene freestanding film provides valuable opportunity not only to tailor the physicochemical properties of the graphene film but also to create unexpected functionality *via* the synergistic coupling between graphene and layered metal oxide components. Yet, at the time of the publication of the present study, we are aware of

I. Y. Kim, S. Park, H. Kim, Prof. S. Park, Prof. S.-J. Hwang
Center for Intelligent Nano-Bio Materials (CINBM)
Department of Chemistry and Nano Sciences
Ewha Womans University
Seoul, 120–750, Korea
E-mail: nanopark@ewha.ac.kr; hwangsju@ewha.ac.kr
Prof. R. S. Ruoff
Department of Mechanical Engineering
and the Materials Science and Engineering Program
The University of Texas at Austin
Austin, TX, 78712, United States

DOI: 10.1002/adfm.201303040

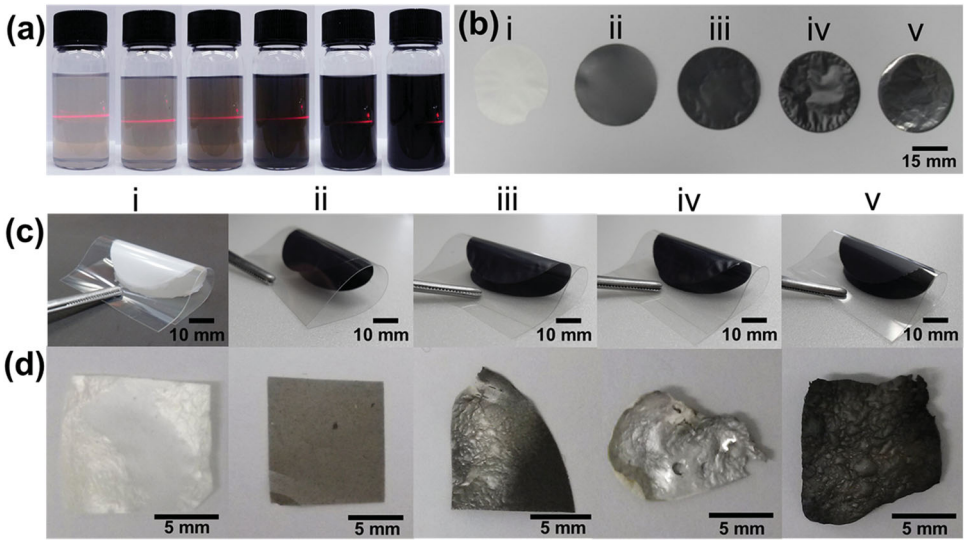

Figure 1. a) Photoimages of the mixture colloidal suspensions of rG-O and layered titanate nanosheets with the $C/Ti_{1.83}O_4$ ratios of 0.2, 0.4, 1, 2, 4, and 8 (from left to right). b) Top-view and c) side-view photoimages of i) pure layered titanate freestanding film, ii) **TG1**, iii) **TG2**, and iv) **TG3**, and v) pure rG-O freestanding film, and d) photos of their microwave-heated derivatives.

no report about the synthesis of freestanding hybrid films composed of rG-O and layered metal oxide nanosheets.

In the present work, an effective methodology to tailor the physicochemical properties of graphene freestanding film is developed by the intimate hybridization of rG-O nanosheets with layered titanate nanosheets. The effects of titanate incorporation on the chemical bonding nature and physicochemical property of the graphene freestanding film are investigated along with the antibacterial activity of the resulting hybrid films for the *Escherichia coli* O157:H7.

2. Results and Discussion

2.1. Fabrication and Stability Tests of the Freestanding Hybrid Films

The mixing of the colloidal suspension of rG-O nanosheets with that of layered titanate nanosheets yields homogeneously mixed suspensions composed of both the nanosheets. The photoimages of a series of mixture colloidal suspensions with the $C/Ti_{1.83}O_4$ molar ratios of 0.2, 0.4, 1, 2, 4, and 8 are illustrated in **Figure 1**a. All of the present mixture colloidal suspensions show a good dispersion ability and high colloidal stability without any phase separation for several weeks, as evidenced by the Tyndall phenomena of the mixture colloidal suspensions. As the content of titanate nanosheets increases, the color of the mixed colloidal suspension becomes brighter. The surface charges of the obtained colloidal suspensions are examined with zeta potential measurements. All of the present suspensions commonly display average zeta potential of –30 to –40 mV, which is compatible with those of the pure suspensions of the rG-O and layered titanate nanosheets (–44 and –29 mV). This finding suggests negligible influence of mixing on the surface charge of each component nanosheet.

The flow-directed filtration of these mixture colloidal suspensions leads to the fabrication of the freestanding hybrid films of rG-O–layered titanate with several $C/Ti_{1.83}O_4$ ratios of 0.4, 1, and 2 (hereafter, these hybrid films are denoted as **TG1**, **TG2**, and **TG3**, respectively), as presented in Figure 1b. As references, the pure freestanding films of layered titanate and rG-O nanosheets are also prepared. As shown in Figure 1c, all of the as-fabricated freestanding films show high flexibility and excellent elastic property. To the best of our knowledge, this is the first example of the freestanding hybrid films consisting of graphene and layered metal oxide nanosheets as well as the freestanding film of layered metal oxide nanosheets. Of prime interest is that the pure titanium oxide freestanding film is highly flexible, strongly suggesting its applicability for flexible electronic devices such as solar cells and electrochromic window (see the Figure S1 in Supporting Information).

As shown in Figure 1d, no morphological evolution of **TG1** occurs upon the microwave heating, which is sharply contrasted with the pure rG-O freestanding film and pure titanate freestanding film experiencing destruction after the same treatment, highlighting the improved stability of the rG-O film upon the incorporation of titanate nanosheets. The enhanced stability of the freestanding hybrid film is further evidenced by the test of ultrasonic stress. While the loading of ultrasonic stress causes severe damage for the pure rG-O film, all the hybrid films of rG-O–layered titanate and pure titanate film do not show any damage by the ultrasonic stress (see the Figure S2 in Supporting Information). Also, the **TG2** and **TG3** hybrid films retain their original structure upon the calcination at 300 °C, which is sharply contrasted with the pure titanate film showing a phase transition to anatase TiO_2. This indicates the stabilization of layered titanate phase by the hybridized rG-O nanosheets (see the Figure S3 in Supporting Information). The remarkable improvements of mechanical strength and chemical stability upon hybridization are

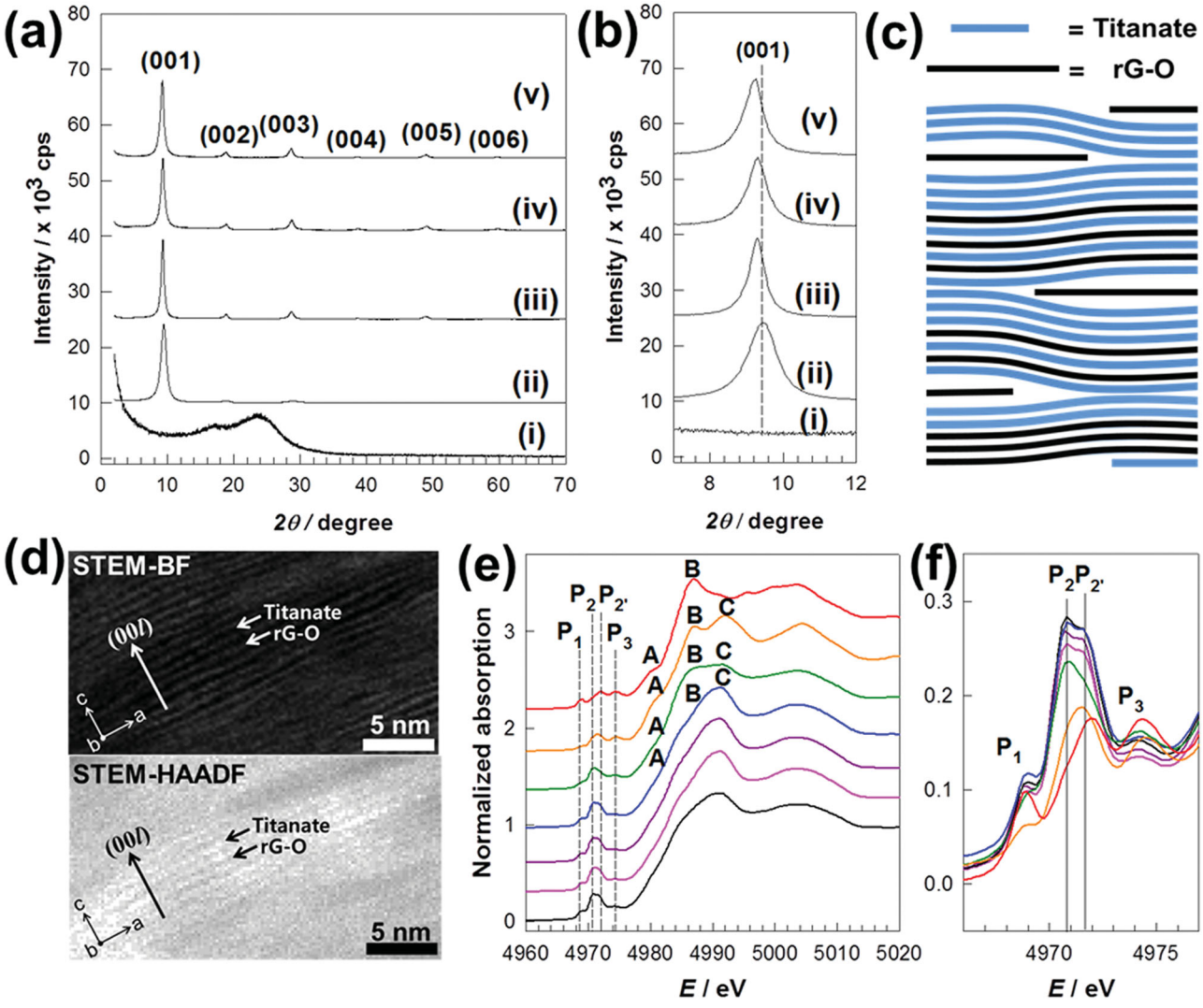

Figure 2. a) XRD patterns of i) the pure rG-O freestanding film, ii) the pure layered titanate freestanding film, iii) **TG1**, iv) **TG2**, and v) **TG3**, and b) the expanded view in the 2θ region of 7–12°. c) Schematic diagram for the stacking structure of the rG-O–layered titanate freestanding hybrid film. d) Cross-sectional STEM–BF and STEM–HAADF images of the **TG1** freestanding hybrid film. e) Ti K-edge XANES spectra for anatase TiO_2 (red), rutile TiO_2 (orange), powdery layered titanate (green), pure layered titanate freestanding film (blue), **TG1** (purple), **TG2** (pink), and **TG3** (black), and (f) their expanded view for pre-edge region.

attributable to strong coupling of two kinds of nanosheets components.

2.2. Local Structure of the Freestanding Hybrid Films

Figure 2a represents the powder X-ray diffraction (XRD) patterns of the rG-O–layered titanate freestanding hybrid films of **TG1**, **TG2**, and **TG3**, as compared with those of pure rG-O and layered titanate freestanding films. While the pure rG-O film shows a weak and broad (*002*) Bragg reflection with a basal spacing of ≈3.49 Å,[3a] the pure layered titanate film and the hybrid films of rG-O-layered titanate exhibit well-developed (*00l*) reflections, indicating the formation of the highly-ordered stacking structure of layered titanate nanosheets with a parallel alignment to the planar direction of the freestanding films. A closer inspection on the present XRD data reveals that the mixing with rG-O nanosheets leads to the low-angle shifts of (*00l*) reflections, indicating the basal expansion of layered titanate lattice (Figure 2b). This finding suggests the fractional invention of graphene nanosheets in the stacking structure of layered titanate nanosheets. According to the least-squares fitting analysis, the basal spacing of the freestanding hybrid films is determined to be c = 9.51, 9.53, and 9.57 Å for **TG1**, **TG2**, and **TG3**, respectively. Regardless of the rG-O/titanate ratios, all freestanding hybrid films including the **TG3** film with the highest rG-O content show similar c-axis lattice parameters that lie in midway between the summation of the theoretical thickness of layered titanate monolayer (~7.00 Å) with the covalent diameter of carbon atom (≈1.52 Å) and that with the van der Waals diameter of carbon atom (≈3.70 Å). This result strongly suggests the existence of significant chemical interactions

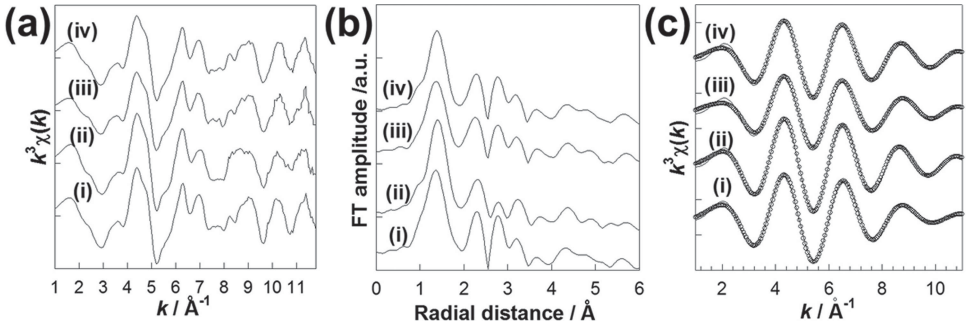

Figure 3. a) Experimental k^3-weighted Ti K-edge EXAFS oscillations, b) their Fourier transformed spectra, and c) their Fourier filtered spectra for i) the pure titanate freestanding film and the rG-O-layered titanate freestanding hybrid films of ii) **TG1**, iii) **TG2**, and iv) **TG3**.

between titanate and rG-O layers in the interstratified stacking structure of the present hybrid films, see the Figure 2c. According to cross-sectional scanning transmission electron microscopy-bright field/scanning transmission electron microscopy-high angle annular dark field (STEM–BF/STEM–HAADF) analysis, the parallel dark lines corresponding to the titanate layers are clearly observed in the STEM–BF image of Figure 2d, indicating the layer-by-layer-ordered stacking of the layered titanate nanosheets. The STEM–HAADF image clearly demonstrates the presence of bright lines between two parallel-aligned dark lines, indicating the formation of the alternating stacking structure of graphene layer with lighter carbon atoms and the titanate layer with heavier atomic weights in some domains. From the viewpoint of entropy, this partially alternating stacking of two kinds of component nanosheets is more favorable than the perfectly interstratified stacking structure. According to micro-Raman spectroscopy (see the Figure S4 in Supporting Information), all the present freestanding hybrid films display characteristic D and G peaks with the similar I_D/I_G ratios of 1.13–1.15, which are somewhat greater than those of powdery rG-O (I_D/I_G = 0.98) and the pure rG-O freestanding film (I_D/I_G = 1.01). This finding suggests that the incorporation of layered titanate nanosheets increases a disorder in the stacking structure of the neighboring rG-O nanosheets. The maintenance of the rG-O species after the fabrication of the freestanding hybrid film is verified by Fourier transformed-infrared (FT-IR) spectroscopy showing only weak features of the oxygenated functional groups (see the Figure S4 in Supporting Information).

According to Ti K-edge X-ray absorption near edge structure (XANES) analysis, both pure titanate freestanding film and freestanding hybrid films show almost identical spectral features, which are nearly identical the *c*-axis-polarized XANES spectra of layered titanate film, see Figure 2e.[7a] In contrast to the powdery reference of layered titanate showing nearly identical intensity for the peaks B and C, the present rG-O–layered titanate hybrid films and the pure titanate film commonly display a larger spectral weight for the peak C than for the peak B. The observed enhancement of the peak C corresponding to the transition from core 1s orbital to in-plane $4p_{x,y}$ one provides direct evidence for the parallel alignment of layered titanate nanosheets to the planar direction of the freestanding films. This finding clearly demonstrates that all the titanate nanosheets are well-ordered in a perpendicular orientation to the planar direction of the freestanding film. The maintenance of original layered structure of titanate nanosheets in the freestanding hybrid films is confirmed by the observation of typical pre-edge spectral features, P_1, P_2, $P_{2'}$, and P_3, of lepidocrocite-type layered titanate phase (Figure 2f).[7]

As shown in **Figure 3**a, all the freestanding films show nearly the same spectral features for the experimental k^3-weighted EXAFS oscillations, confirming the identical local structure and orientation of the titanate nanosheets in these materials. All of the freestanding films demonstrate longer (Ti–O) bond distances than does the pure layered titanate freestanding film in the Fourier transforms (FT) of the k^3-weighted EXAFS data, see Figure 3b. To quantitatively determine the local structure of titanate layers in the present freestanding films, the first FT peak corresponding to (Ti–O) bonds is isolated by inverse Fourier transformation (i.e., Fourier filtering, FF) to k space and then curve-fitted. The resulting $k^3\chi(k)$ FF EXAFS data are shown in Figure 3c, together with the calculated data. All of the present FF data are well-reproduced with the structural model of lepidocrocite-type layered titanate, confirming the maintenance of the original crystal structure of layered titanate nanosheets after the formation of freestanding films.

As presented **Table 1**, the observed elongation of (Ti–O) bond distance upon hybridization strongly suggests an increase of the electron density in the layered titanate nanosheets by the sharing of π-electron clouds in the hybridized rG-O nanosheets. The present finding can be regarded as strong evidence for the strong chemical interaction between rG-O and layered titanate nanosheets. The coordination numbers of the (Ti–O) coordination shells are somewhat smaller for all the hybrid films than for the pure layered titanate film, reflecting the elastic deformation of titanate layers by the intervened rG-O nanosheets in the hybrid films.

2.3. Antibacterial Activity of the Freestanding Hybrid Films

Since the graphene freestanding film is reported to possess a good antibacterial activity,[4] the effect of the incorporation of titanate nanosheets on the antibacterial activity of the pure graphene freestanding film is investigated. As plotted in **Figure 4**a, all the rG-O-layered titanate freestanding hybrid films as well as pure

Table 1. Results of non-linear least-squares curve fittings for the polarized Ti K-edge EXAFS spectra for the rG-O-layered titanate freestanding hybrid films of **TG1**, **TG2**, and **TG3**, and the pure titanate freestanding film.

Sample	Bond	CN	R [Å]	σ^2 [$10^{-3} \times$ Å^2]
Pure titanate film[a)]	$(Ti–O)_1$	2	1.84	5.01
	$(Ti–O)_2$	2	1.93	
	$(Ti–O)_3$	2	2.02	
Hybrid film **TG1**[b)]	$(Ti–O)_1$	1.7	1.87	3.97
	$(Ti–O)_2$	1.7	1.95	
	$(Ti–O)_3$	1.7	2.05	
Hybrid film **TG2**[c)]	$(Ti–O)_1$	1.4	1.88	3.52
	$(Ti–O)_2$	1.4	1.95	
	$(Ti–O)_3$	1.4	2.07	
Hybrid film **TG3**[d)]	$(Ti–O)_1$	1.5	1.88	3.25
	$(Ti–O)_2$	1.5	1.96	
	$(Ti–O)_3$	1.5	2.08	

The curve fitting analysis was performed for the range of [a)]0.951–*R*–1.933 Å and 2.10–*k*–12.25 Å^{-1}; [b)]0.920–*R*–1.933 Å and 2.10–*k*–12.10 Å^{-1}; [c)]0.951–*R*–1.994 Å and 2.05–*k*–11.80 Å^{-1}, 0.951–*R*–1.963 Å, and [d)]2.10–*k*–12.15 Å^{-1}. ΔR is ±0.01 Å.

layered titanate freestanding film exhibit complete sterilization effects to *E. coli* cells only in 15 min, which is the strongest sterilization activity among reported nanostructured carbon-based antibacterial films.[4,8,9] The **TG1** freestanding film with the highest antibacterial activity induces a remarkable decrease of the viable cell number from 2.95×10^7 cells mL^{-1} to 6.3×10^3 cells mL^{-1}, indicating 99.98% antibacterial activity within 5 min. This activity is much stronger than those of the **TG2** and **TG3** freestanding films as confirmed by low p value (t-test) of <0.0001.[10] Eventually after 15 min, no viable *E. coli* cells are detectable on the surface of the hybrid films. Although the antibacterial activity for *E. coli* cells also occurs for the pure rG-O freestanding film, the antibacterial activity of this film is significantly weaker than those of the hybrid films. There are three kinds of sterilization mechanisms responsible for the antibacterial activity of the graphene freestanding film, that is, a membrane stress (i.e., a direct physical contact between graphene and bacteria that leads to membrane perturbation and to the release of intracellular contents),[4a,11a] a reactive oxygen species (ROS)-dependent oxidative stress,[11b] and a ROS-independent oxidative stress.[4b]

As presented in the field emission-scanning electron microscopy (FE-SEM) images of Figure 4b, the pure rG-O and layered titanate freestanding film shows a flat and clean surface, whereas the freestanding hybrid films of rG-O-layered titanate display sharp edges on their surface, which is attributable to the formation of stacking faults between two different kinds of rG-O and layered titanate nanosheets. The homogeneous distribution of C and Ti elements in the entire parts of the present films is evidenced by cross-sectional elemental mapping analysis and energy dispersive spectrometry (EDS) analysis, see the Figure S5 in Supporting Information. Also no phase separation of rG-O and titanate nanosheets is observable during the fabrication of the present hybrid films. On the basis of these findings, the surface layer of the freestanding hybrid films is supposed to possess identical rG-O/layered titanate ratios to the initial mixing ratios of two precursor nanosheets. In the case of **TG1**, the sharp edges density is even greater than those of **TG2** and **TG3**. As demonstrated in the inset of Figure 4b, the presence of sharp edges leads to the smaller contact angle of water droplet on the surface of the freestanding hybrid films than those of layered titanate freestanding film and rG-O freestanding film, reflecting the remarkably enhanced hydrophilic nature of the rG-O–layered titanate freestanding hybrid films. The FE-SEM analysis for

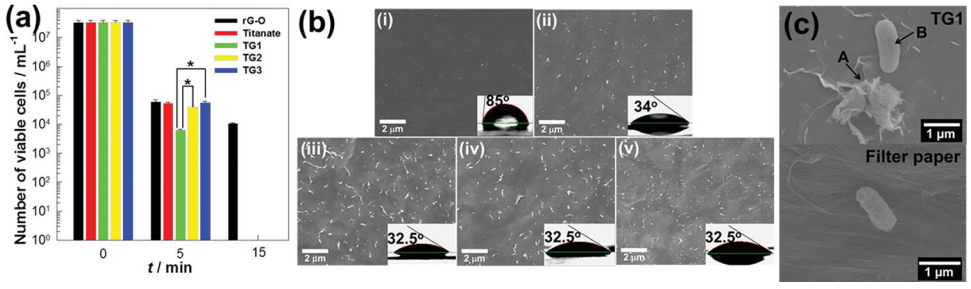

Figure 4. a) Time-dependent variation of the number of viable *E. coli* cells dropped on **TG1** (green), **TG2** (yellow), and **TG3** (blue), and pure rG-O freestanding film (black) and pure layered titanate freestanding film (red). Graph data presentation: ± standard deviation. *p-value (t-test) < 0.0001. b) FE-SEM images of i) pure rG-O freestanding film, ii) pure layered titanate freestanding film, iii) **TG1**, iv) **TG2**, and v) **TG3**. Inset shows the contact angle of water droplet on the films. c) FE-SEM images of *E. coli* cells on the **TG1** and the filter paper after an exposure for 15 min.

Table 2. Generation test of ROS and oxidation test of GSH for the rG-O–layered titanate freestanding hybrid films of **TG1**, **TG2**, and **TG3**, the pure layered titanate freestanding film, and the pure rG-O freestanding film.

	Generation test of ROS		Oxidation test of GSH	
Sample	Abs. at 470 nm	Formation of XTT-formazan by ROS	Abs. at 412 nm	Loss of GSH% [a]
Titanate film	0.008	Negligible	0.561	12.5
Hybrid film **TG1**	0.008	Negligible	0.536	16.4
Hybrid film **TG2**	0.008	Negligible	0.501	21.8
Hybrid film **TG3**	0.007	Negligible	0.501	21.8
rG-O film	0.006	Negligible	0.464	27.6
Negative control[b]	–	–	0.641	–
Positive control[c]	–	–	0.130	79.7

[a]Loss of GSH% = (absorbance of negative control – absorbance of sample)/absorbance of negative control × 100; [b]GSH solution without film was used as a negative control; [c]GSH (0.4 mm) oxidization by H_2O_2 (1 mm) was used as a positive control.

the *E. coli* cells exposed on the **TG1** hybrid freestanding film demonstrates the irreversible destruction (denoted as A) by the edges of nanosheets, which is sharply contrasted to no damage of the *E. coli* cell on the filter paper (Figure 4c). This finding strongly suggests a significant contribution of membrane stress mechanism. Also the enhanced adhesion of bacteria on the rough surface of freestanding hybrid films makes additional contribution to the excellent antibacterial activity of the freestanding hybrid films. For the other *E. coli* cell on the freestanding hybrid films (denoted as B), the formation of hollow surface defect is discernible, suggesting the additional contribution of oxidative stress.[11a]

As summarized in **Table 2**, the contributions of the two kinds of oxidative stress mechanisms, that is, the ROS-dependent and the ROS-independent oxidative stress, are probed with the tests of the generation of ROS and the oxidation of glutathione (GSH). All of the present films including **TG1**, **TG2**, and **TG3** do not show experimental evidence for the significant generation of ROS, highlighting the negligible contribution of the ROS mechanism to the observed high antibacterial activity of the present freestanding hybrid films. Conversely, the oxidation of GSH occurs for all the present freestanding films, suggesting the significant contribution of ROS-independent oxidative stress to the activity of all the present films. However, the oxidation of GSH is weaker for the hybrid films than for the pure rG-O film, which is contrasted with the higher antibacterial activity of the formers than the latter. This finding clearly demonstrates that ROS-independent oxidative stress is not mainly responsible for the enhancement of the antibacterial activity of the rG-O film upon the incorporation of layered titanate nanosheets.

Taking into account the photocatalytic activity of titanate nanosheet, it is highly probable that the photoinduced antibacterial activity of titanate component would make additional contribution to the observed excellent antibacterial functionality of the present hybrid films. To experimentally confirm this possibility, an additional test of antibacterial property is carried out for all the present hybrid films with the illumination of UV and visible light. However, the very high antibacterial activity of these films makes impossible this test. That is, all the *E. coli* cells are killed during the drying process of the films for the photo-induced antibacterial activity test.

3. Conclusion

In summary, an effective method to tailor the physicochemical properties and antibacterial functionality of graphene freestanding film is obtained by the incorporation of titanate nanosheets. The freestanding hybrid films of rG-O and layered titanate exhibit greater mechanical strength, higher chemical stability, and greater hydrophilicity than do rG-O freestanding films. Of prime importance is that these hybrid films display unexpected high sanitization efficiency of 100% only within 15 min, which is much superior to any other nanostructured carbon-based films. The incorporation of titanate nanosheets provides powerful way of controlling the surface roughness and membrane stress of graphene film, leading to the dramatic enhancement of its antibacterial property. The universal applicability of the present synthetic strategy is obviously evidenced by the fabrication of rG-O-layered MnO_2 freestanding hybrid film *via* the same filtration process of the colloidal mixtures of rG-O and layered MnO_2 nanosheets (see the Figure S6 in Supporting Information).

4. Experimental Section

Sample Preparation: The homogeneously mixed suspensions of rG-O and layered titanate nanosheets were synthesized by adding the rG-O suspension into the layered titanate suspension, which was followed by a dialysis with 0.5 wt% aqueous ammonia solution. The freestanding hybrid films of rG-O-layered titanate were fabricated by the flow-directed filtration of the resulting mixed colloidal suspension through an Anodisc membrane filter.

Antibacterial Activity Tests: *E. coli* O157:H7 (43894) was obtained from ATCC (Gaithersburg, MD, USA). The antibacterial activity was investigated by the drop test method with some modification.[9] 1 μL of PBS containing *E. coli* cells (≈2.95×10^7 cells·mL^{-1}) was dropped on a film. Four drops were separately located at different sites of each film. After the exposure of the film for 0, 5, and 15 min in dark at room temperature, the surface of the film was washed with PBS. The number of live *E. coli* cells in PBS was estimated by counting colonies on LB agar plates through a serial 10-fold dilution and incubating cells at 37 °C for 24 h.

Supporting Information

Supporting Information is available from the Wiley Online Library or from the author.

Acknowledgements

This work was supported by the Core Technology of Materials Research and Development Program of the Korea Ministry of Intelligence and Economy (grant No. 10041232) and by Korea Ministry of Environment as "Converging Technology Project" (191–101–001). The experiments at PAL were supported in part by MOST and POSTECH. S.P. and H.K. are thankful for the financial support by the Public welfare & safety research program (2012M3A2A1051681).

Received: August 30, 2013
Revised: October 30, 2013
Published online: December 12, 2013

[1] a) A. K. Geim, K. S. Novoselov, *Nat. Mater.* **2007**, *6*, 183; b) D. Li, M. B. Müller, S. Gilje, R. B. Kaner, G. G. Wallace, *Nat. Nanotechnol.* **2008**, *3*, 101; c) I. Khrapach, F. Withers, T. H. Bointon, D. K. Polyushkin, W. L. Barnes, S. Russo, M. F. Craciun, *Adv. Mater.* **2012**, *24*, 2844.

[2] a) D. A. Dikin, S. Stankovich, E. J. Zimney, R. D. Piner, G. H. B. Dommett, G. Evmenenko, S. T. Nguyen, R. S. Ruoff, *Nature* **2007**, *448*, 457; b) J. N. Coleman, M. Lotya, A. O'Neill, S. D. Bergin, P. J. King, U. Khan, K. Young, A. Gaucher, S. De, R. J. Smith, I. V. Shvets, S. K. Arora, G. Stanton, H.-Y. Kim, K. Lee, G. T. Kim, G. S. Duesberg, T. Hallam, J. J. Boland, J. J. Wang, J. F. Donegan, J. C. Grunlan, G. Moriarty, A. Shmeliov, R. J. Nicholls, J. M. Perkins, E. M. Grieverson, K. Theuwissen, D. W. McComb, P. D. Nellist, V. Nicolosi, *Science* **2011**, *331*, 568; c) A. R. Ranjbartoreh, B. Wang, X. Shen, G. Wang, *J. Appl. Phys.* **2011**, *109*, 014306.

[3] a) H. Chen, M. B. Müller, K. J. Gilmore, G. G. Wallace, D. Li, *Adv. Mater.* **2008**, *20*, 3557; b) R. R. Nair, H. A. Wu, P. N. Jayaram, I. V. Grigorieva, A. K. Geim, *Science* **2012**, *335*, 442; c) S. Li, Y. Luo, W. Lv, W. Yu, S. Wu, P. Hou, Q. Yang, Q. Meng, C. Liu, H.-M. Cheng, *Adv. Energy Mater.* **2011**, *1*, 486; d) J. Lu, Y.-S. He, C. Cheng, Y. Wang, L. Qiu, D. Li, D. Zou, *Adv. Funct. Mater.* **2013**, *23*, 3494; e) F. Xiao, Y. Li, X. Zan, K. Liao, R. Xu, H. Duan, *Adv. Funct. Mater.* **2012**, *22*, 2487; f) X. Wang, X. Cao, L. Bourgeois, H. Guan, S. Chen, Y. Zhong, D.-M. Tang, H. Li, T. Zhai, L. Li, Y. Bando, D. Golberg, *Adv. Funct. Mater.* **2012**, *22*, 2682.

[4] a) W. Hu, C. Peng, W. Luo, M. Lv, M. Li, X. Li, D. Li, Q. Huang, C. Fan, *ACS Nano* **2010**, *4*, 4317; b) S. Liu, T. H. Zeng, M. Hofmann, E. Burcombe, J. Wei, R. Jiang, J. Kong, Y. Chen, *ACS Nano* **2011**, *5*, 6971.

[5] a) J. K. Lee, K. B. Smith, C. M. Hayner, H. H. Kung, *Chem. Commun.* **2010**, *46*, 2025; b) J. Liang, Y. Xu, D. Sui, L. Zhang, Y. Huang, Y. Ma, F. Li, Y. Chen, *J. Phys. Chem. C* **2010**, *114*, 17465; c) C. Yuan, L. Yang, L. Hou, J. Li, Y. Sun, X. Zhang, L. Shen, X. Lu, S. Xiong, X. W. Lou, *Adv. Funct. Mater.* **2012**, *22*, 2560; d) N. Li, G. Zhou, R. Fang, F. Li, H.-M. Cheng, *Nanoscale* **2013**, *5*, 7780.

[6] a) D. G. H. Ballard, G. R. Rideal, *J. Mater. Sci.* **1983**, *18*, 545; b) J. J. Kellar, Functional Fillers and Nanoscale Minerals: New Markets/New Horizons, Society for Mining, Metallurgy and Exploration, Littleton, Colorado, **2006**; c) I. Y. Kim, J. M. Lee, T. W. Kim, H. N. Kim, H. I. Kim, W. Choi, S.-J. Hwang, *Small* **2012**, *8*, 1038; d) D.-Y. Sung, T. W. Kim, J. L. Gunjakar, I. Y. Kim, Y. R. Lee, S.-J. Hwang, *Chem. Eur. J.* **2013**, *19*, 7109.

[7] a) K. Fukuda, I. Nakai, C. Oishi, M. Nomura, M. Harada, Y. Ebina, T. Sasaki, *J. Phys. Chem. B* **2004**, *108*, 13088; b) S. G. Hur, D. H. Park, T. W. Kim, S.-J. Hwang, *Appl. Phys. Lett.* **2004**, *85*, 4130.

[8] a) J. Ma. J. Zhang, Z. Xiong, Y. Yong, X. S. Zhao, *J. Mater. Chem.* **2011**, *21*, 3350; b) L. Brunet, D. Y. Lyon, E. M. Hotze, P. J. J. Alvarez, M. R. Wiesner, *Environ. Sci. Technol.* **2009**, *43*, 4355.

[9] O. Akhavan, E. Ghaderi, *J. Phys. Chem. C* **2009**, *113*, 20214.

[10] *p*-value (*t*-test) < 0.0001 between the **TG1** and **TG2** or **TG1** and **TG3** means that the resulting value of **TG1** is 99.99% variant from that of **TG2** and **TG3**, respectively.

[11] a) C. D. Vecitis, K. R. Zodrow, S. Kang, M. Elimelech, *ACS Nano* **2010**, *4*, 5471; b) E. Cabiscol, J. Tamarit, J. Ros, *Int. Microbiol.* **2000**, *3*, 3.